

Analyst

Accepted Manuscript



This is an *Accepted Manuscript*, which has been through the Royal Society of Chemistry peer review process and has been accepted for publication.

Accepted Manuscripts are published online shortly after acceptance, before technical editing, formatting and proof reading. Using this free service, authors can make their results available to the community, in citable form, before we publish the edited article. We will replace this *Accepted Manuscript* with the edited and formatted *Advance Article* as soon as it is available.

You can find more information about *Accepted Manuscripts* in the [Information for Authors](#).

Please note that technical editing may introduce minor changes to the text and/or graphics, which may alter content. The journal's standard [Terms & Conditions](#) and the [Ethical guidelines](#) still apply. In no event shall the Royal Society of Chemistry be held responsible for any errors or omissions in this *Accepted Manuscript* or any consequences arising from the use of any information it contains.



Analyst

ARTICLE

Single-Molecule Visualization of ROS-induced DNA Damage in Large DNA Molecules

Jinyong Lee,^a Yongkyun Kim,^a Sangyong Lim^b and Kyubong Jo^{*a}Received 00th January 20xx,
Accepted 00th January 20xx

DOI: 10.1039/x0xx00000x

www.rsc.org/

We present a single molecule visualization approach for the quantitative analysis of reactive oxygen species (ROS) induced DNA damage, such as base oxidations and single stranded breaks in large DNA molecules. We utilized Fenton reaction to generate DNA damage with subsequent enzymatic treatment using the mixture of three types of glycosylases to remove oxidized bases, and then fluorescent labeling on damaged lesions *via* nick translation. This single molecule analytical platform provided the capability to count one or two damaged sites per λ . DNA molecule (48.5 kb), which were reliably dependent on the concentrations of hydrogen peroxide and ferrous ion at micromolar level. More importantly, labeled damaged sites that were visualized under a microscope provided positional information, which offered the capability of comparing DNA damaged sites with *in silico* genomic map to reveal sequence specificity that GTGR is more sensitive to oxidative damage. Consequently, single DNA molecule analysis provides the sensitive analytical platform for ROS-induced DNA damage and suggests an interesting biochemical insight that genome primarily active during the prophage may have less probability for oxidative DNA damage.

Introduction

Single molecule analysis is attractive because it can dramatically reduce the limits of detection, such that it is approaching quantification of individual molecular events instead of simply determining molar concentrations. Furthermore, single molecule measurement provides additional information that is not expected in ensemble average measurement. In particular, long and linear DNA molecules are a versatile platform for a variety of analyses because it is possible to directly visualize biochemical events on elongated DNA backbones within microfluidic devices, including functionalized surfaces and nanostructures.¹ Elongated large DNA molecules have primarily been utilized for the development of a number of genome analysis platforms²⁻⁴ but also for the study of polymer physics.⁵⁻⁷ Importantly, single DNA molecule approaches have a unique advantage for stochastic random biochemical event analysis, such as DNA damage⁸ and DNA-protein interactions,⁹ because they can provide information that may not be apparent in bulk biochemical assays.

Previously, we introduced the visualization approach for ultraviolet-induced DNA damage in large genomic DNA molecules by fluorescent labelling using nick translation.⁸ Our scheme was applied to another type of damage such as

reactive oxygen species (ROS)-induced DNA damage.¹⁰ These previous studies proved the concept of single-molecule application that could be applied for DNA damage analysis, and they implied a potential for single molecule approach to be a powerful tool for investigating fundamental mechanisms and characteristics of DNA damage.

ROS-induced DNA damage is of considerable interest because oxidative DNA damage is implicated in a number of important biological processes, such as ageing,¹¹ and various diseases, including cancer.^{12, 13} Reactive oxygen species are unavoidable because they are produced endogenously from normal cellular metabolism¹⁴ as well as exogenously from the environment. For example, reactive oxygen species are generated from inhaled oxygen (O₂). According to Fenton's reaction,¹⁵ iron or other metal ions within cells converts oxygen to active oxygen radicals, such as •OH, •HO₂, and H₂O•, which are the primary cause of oxidative DNA damage through radical attack.¹⁶ Reactive oxygen species can also attack any type of biomolecule in our body. However, these molecules including lipids and proteins are rapidly replaced during normal cellular maintenance. In contrast, DNA damage is a critical biological issue because it is difficult to recover lost information stored in DNA. Despite numerous DNA repairing machineries in cells, cumulative DNA damage over time still contributes to ageing and various diseases. For example, it is well-known that each cell in a 70 year old human has about 2,000 scars of sequence information lost by non-homologous end joining.¹⁷

Imlay *et al.* pioneered the study of ROS-induced DNA toxicity using the Fenton reaction *in vivo* and *in vitro*.¹⁸ A number of studies followed to develop several methods for

^a Department of Chemistry and Interdisciplinary Program of Integrated Biotechnology, Sogang University, Seoul, Korea, 121-742.

^b Research Division for Biotechnology, Korea Atomic Energy Research Institute, Jeongseup, Korea, 580-185.

Electronic Supplementary Information (ESI) available.
See DOI: 10.1039/x0xx00000x

detecting ROS-induced DNA breaks, such as alkaline elution,¹⁹ comet assay,^{20, 21, 32} *p*-postlabeling methods,^{22, 23} and AFM.²⁴ Chemical modifications of DNA damage have also been identified *via* chromatography-coupled mass spectrometry.²⁵ Specifically, 8-oxo-dG is used as an oxidative damage marker because it can be detected in the femtomolar range by electrochemical HPLC.^{27, 28} Nonetheless, there is a need for more advanced methods to detect ROS-induced DNA damage. For example, diseases that result from ROS-induced DNA damage generally arise long after the DNA damage has occurred; the effect is due to a chronic accumulation rather than an acute event. Thus, it is very difficult to identify ROS-induced DNA damage until sufficient damage has accumulated to cause a disease.

In this context, single molecule analysis is a powerful tool for sensitively detecting ROS-induced DNA damage because this approach can directly detect damaged lesions in individual DNA molecules that would be masked in other bulk assays. Although a proof-of-concept experiment was conducted for single molecule visualization of ROS-induced DNA damage in human cancer cell,¹⁰ cellular response was too much complicated to explain ROS-induced DNA damage itself because it is not easy to control and understand numerous DNA repairing processes in a human cell. Instead, here we focused on DNA molecule itself, which directly responds to ROS with quantitative dependence on the concentration of H₂O₂ and Fe²⁺. More importantly, we investigated the correlation between DNA sequence and ROS-induced damage within the genomic map without cellular responses.

Experimental Section

Chemicals

Endonuclease III (Nth), endonuclease VIII (Nei), Fpg (formamidopyrimidine DNA glycosylase), and deoxynucleoside triphosphates (dNTP) were purchased from New England Biolabs (Ipswich, MA). DNA polymerase I was purchased from Roche Applied Sciences (Indianapolis, IN). Alexafluor 647-aha-dUTPs were purchased from Thermo Fisher Scientific (Waltham, MA). All other chemicals were obtained from Sigma-Aldrich (St. Louis, MO).

λ phage DNA preparation

Escherichia coli bacteriophage λ (ATCC 23724-B2) was obtained from ATCC (Manassas, VA), and was propagated in the bacterial host *Escherichia coli* C600 (ATCC 23724) in TNT broth (Tryptone, Sodium chloride and Thiamine media) to a titer of 10⁶ PFU/ μ L. Cell culture and phage propagation followed the ATCC protocol. Bacteriophage λ was prepared fresh for each experiment. λ DNA was extracted using proteinase K in 10 mM potassium phosphate buffer (pH 7.4), for one hour at 65 °C in a water bath.

DNA immobilization and elongation

Microfluidic channels (height: 5 μ m \times width: 100 μ m) in a polydimethylsiloxane (PDMS) device were mounted on a

positively charged glass surface, and then the solution of DNA molecules (2 ng/ μ L) were loaded onto the entrance of the microfluidic channels. As the solution moved through the microfluidic channels by capillary action, DNA molecules were elongated and deposited on the positively charged surface. To prevent DNA desorption from the surface during chemical reactions, a thin layer of acrylamide (3.3%) was added to the surface and cured.²⁹

DNA damage via Fenton's reaction.

Ferrous chloride (FeCl₂) and hydrogen peroxide (H₂O₂) solutions were prepared fresh for each treatment. Various concentrations of the ferrous chloride solution were applied to the surface-bound DNA for 5 min (Fig. 1a). To generate hydroxyl radical with ferrous ions, hydrogen peroxide was added on the acrylamide layer and incubated for 30 min at 37 °C. After incubation, the surface was washed twice with 0.5 mL of 1 \times TE buffer solution. For location analysis of damaged lesions in λ DNA molecule, restriction enzyme *Xho*I (10 units) in 200 μ L Cutsmart buffer (50 mM Potassium Acetate, 20 mM Tris-acetate, 10 mM Magnesium Acetate, 100 μ g/ml BSA, pH 7.9, NEB) was added before ferrous chloride and hydrogen peroxide treatment.

Labelling damaged DNA.

To label ROS induced DNA damage, we prepared a repair enzyme mix containing 10 unit Nth (Endonuclease III), 10 unit Nei (Endonuclease VIII), 8 unit Fpg, 5 unit DNA polymerase I, 100 μ M dNTP mix (dATP, dCTP, dGTP), 10 μ M dTTP and 10 μ M Alexafluor 647-aha-dUTP in NEB buffer 2 (50 mM NaCl, 10 mM Tris-HCl, 10 mM MgCl₂, 1 mM DTT, pH 7.9). On each glass surface, 0.2 mL of repair enzyme mix solution was added and incubated in a humidified chamber at 37 °C for 1 hr. Comparing to our previous method,⁸ nucleotide concentration was reduced to one tenth (e.g. from 1 mM dATP to 0.1 mM, from 100 μ M Alexafluor-647-labeled dUTP to 10 μ M) because of smaller amount of DNA that was immobilized on the surface. In addition, we utilized only one type of Alexafluor 647 labeled dUTP without fluorescent-labeled dCTP through optimization. After damaged site labelling, the surface was washed twice with 0.5 mL of 1 \times TE buffer solution and then stained with 5 μ L of 0.1 mM YOYO-1 with 1 % β -mercaptoethanol (anti-bleaching agent).

DNA visualization and data acquisition

An inverted microscope (Zeiss Observer A1, AG, Germany) was equipped with a 63 \times Zeiss Plan-Neofluar oil immersion objective illuminated by a solid-state laser (Coherent Sapphire 488, Santa Clara, CA). Fluorescence images were captured by an electron multiplying charge-coupled device digital camera (EMCCD: Evolve, Roper Scientific, Tucson, AZ) and stored in 16-bit TIFF format generated by RS Image (Roper Scientific). For FRET (Fluorescent Resonance Energy Transfer) imaging,^{3, 8} two emission filters were used: an emission filter for the green channel (holographic notch filter for 488 nm, Namil Optical Components Corp, Incheon, Korea) and another for the red

channel (XF3076; Omega Optical, Inc., Brattleboro, VT). The green channel acquired DNA backbones stained with YOYO-1 (509 nm, emission), while the red FRET imaged AlexaFluor 647 (665 nm emission) spots. For localization of red FRET punctate analysis, two images from the green channel and red channel were merged and corresponding label spot positions were determined against background using DNA length profiles in ImageJ. Subsequently, we counted the total number of Alexafluor-647 labelled red dots on stretched λ DNA molecules, and divided into total number of λ DNA molecules in a single image. Each image has 100 to 300 DNA molecules. Data were statistically analysed, using a one-way analysis at variance (ANOVA), followed by the Student-Neuman-Keuls' test. The level of $p < 0.05$ was accepted as statistically significant.

Results and discussion

Figure 1a illustrates a schematic to visualize ROS-induced DNA damage *via* fluorescent labelling. In this method, large DNA molecules were first elongated and immobilized onto trimethoxy silane coated positively charged glass surface *via* capillary action within a microfluidic device.²⁹ The immobilized DNA molecules were treated with FeCl_2 and H_2O_2 . The oxidized bases were then removed enzymatically with a mix of glycosylases, leaving a baseless sugar (AP site: apurinic or apyrimidinic site), which were converted into nicks by AP lyase activity of glycosylases. DNA polymerase I was then used to incorporate Alexafluor-647-labeled dUTPs into the DNA.⁸ Finally, DNA molecules were stained with the intercalating dye YOYO-1 for visualization by fluorescent microscope imaging using FRET (fluorescence resonance energy transfer): YOYO-1 was the FRET donor and Alexafluor-647 was the FRET acceptor.³

Figure 1b shows representative fluorescence micrographs of single DNA molecules with ROS-induced damage at increasing H_2O_2 concentrations. An advantage of single molecule DNA damage analysis is that we only need small amount of sample for quantitative analysis compare with other conventional methods, since statistical analysis is possible with DNA molecules that we can count. Therefore, we analysed hundreds of DNA molecules from micrographs, to count red fluorescent labels on DNA backbones for damage quantification.

However, it is noticeable that red spots have different sizes. To explain this size difference, it is necessary to understand characteristics of nick translation. DNA polymerase binds a nick and incorporates many nucleotides with and without fluorochrome. Although, in a typical physiological condition, DNA polymerase I synthesizes 15 to 20 nucleotides in a single processive activity,³⁰ DNA polymerase I has different processivity depending on nucleotide concentrations and base compositions.⁹ For example, it can synthesize 400 nucleotides with high concentrations of nucleotides, particularly *in vitro* condition.³¹ In addition, it is possible that multiple polymerases bind the same nick successively. In other words, a

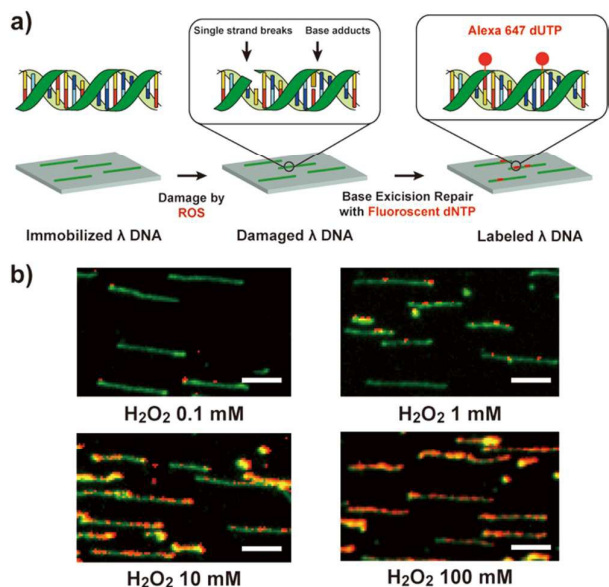


Figure 1. a) Schematic of single molecule Fenton reaction induced DNA damage analysis. Glycosylases excise damaged lesions in elongated λ DNA (48.5 kb), and DNA polymerase I incorporates Alexafluor-647 dUTP into these sites. b) Fluorescent images of labelled DNA with 0.1 mM FeCl_2 , and H_2O_2 from 0.1 mM, to 100 mM. The DNA backbones were stained with YOYO-1 (green) and damaged sites were labelled with Alexafluor-647 dUTP (red). (Scale bar: 5 μm).

polymerase continues synthesis on the DNA that another polymerase finished synthesis. We often observed that overnight nick translation reaction generates red-colour DNA backbones due to multiple DNA polymerases reactions. Therefore, different processivity and multiple DNA polymerases explain why different spot sizes were formed in Fig. 1b. The long processivity and multiple polymerases binding also restrict the analysis of adjacent damaged lesions that would be merged by polymerase reaction.

Furthermore, if two labelled spots were located too closely, it could not be resolved due to the diffraction limit.³² Figure 1b shows that when the concentration of H_2O_2 is higher than 1 mM, there are too many fluorescent labels to distinguish individual spots. Therefore, our DNA damage quantification was restricted to low hydrogen peroxide concentrations (< 1 mM) in order to prevent adjacent labelled spots from overlapping. We assumed that if H_2O_2 were less than 1 mM, the probability for two overlapped spots would be very low because there were only a few labelled spots per λ DNA molecule (Fig. 1b). More importantly, sub-millimolar range is relevant to physiological condition.³³ For example, *E. coli* cells endogenously generate 14 $\mu\text{M}/\text{sec}$ ROS during glucose metabolism, though the steady state concentration does not exceed 20 nM.³⁴ For human body, the concentrations are not uniform, but generally less than 100 μM .³⁵

Figure 2 demonstrates quantitative analysis for Fenton reaction induced DNA damage treated with three glycosylases respectively and their mixture. First, we would like to confirm how many nicks existed intrinsically right after DNA purification.

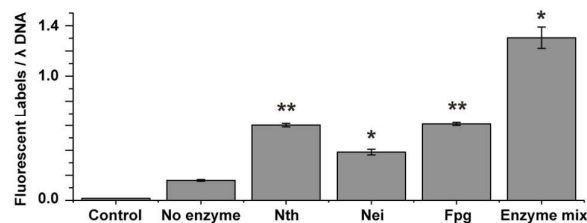


Figure 2. Glycosylase dependence on Fenton reaction induced DNA damage. Fenton reaction was performed with 100 μM FeCl_2 and 100 μM H_2O_2 . The control represents intrinsic nicks existing in purified λ DNA without Fenton reaction (0.016). No enzyme represents Fenton reaction induced single stranded breaks without enzyme treatment. Nth is *E. coli* endonuclease III, Fpg is *E. coli* formamidopyrimidine-DNA-glycosylase, and Nei is *E. coli* endonuclease VIII. Enzyme mix represents the mixture of three enzymes. Each experimental data point represents measurement from 100 to 300 molecules; error bars represent standard deviation for three independent trials. Asterisks indicate the significance comparing with no enzyme experiment (* $p < 0.05$, ** $p < 0.01$).

Among 122 λ DNA molecules harvested from phage propagation, we found only two labelled spots after nick translation, which was 0.016 labels/ λ DNA. This value was significantly smaller than other experimental results in this paper. Therefore, λ DNA directly extracted from bacteriophage was an optimal basis for *in vitro* DNA damage analysis.

Fenton reaction (100 μM H_2O_2 and 100 μM Fe^{2+}) itself generates nicks without enzyme treatment as shown Fig. 2. However, the number of labelled spots increased significantly after glycosylase treatment. Because *E. coli* cells *in vivo* use three types of glycosylases, we used three enzymes in this study: endonuclease III (Nth), endonuclease VIII (Nei), formamido-pyrimidine-DNA-glycosylase (Fpg).³⁶ Nth excises oxidized pyrimidines.³⁷ Nei and Fpg excise oxidized purines such as 8-oxo-dG.^{38, 39} However, Fpg treatment produced more labels than Nei, which implied their different functions (Figure 2). Interestingly, the number of DNA damage from enzyme mix treatment was smaller than simple addition of the number of labels from three enzymes, which suggested that some enzymatic functions overlapped, though their functions were not exactly the same. Nonetheless, since a single type of glycosylase did not cover all kinds oxidative damage, we primarily utilized the mixture of these three enzymes.

Oxidative damage by the Fenton reaction is dependent on the concentration of H_2O_2 and Fe^{2+} . Figure 3a shows that the increase of H_2O_2 concentrations from 0.1 μM to 1 mM generates more damaged sites up to 1.8 per λ DNA molecule at 100 μM Fe^{2+} . The difference for DNA damage was almost negligible below 1 μM H_2O_2 . For Fe^{2+} concentration, we chose sub-100 μM as shown in Fig. 3b since most physiological concentrations are in this range. For example, free iron in an *E. coli* cell ranges from 20 μM to 100 μM .³³ Human serum also has 20 to 30 μM , though liver has 6.3 mM.⁴⁰ Figure 3b shows a quantitative trend of the number of oxidative damaged sites with increasing Fe^{2+} concentration.

A large DNA molecular platform has another powerful capability to obtain genome-specific information by physically mapped DNA.^{2, 41} For example, we previously analysed sequence dependence of UV-induced DNA damage compared with thymine dimer (TT) frequency *in silico* map.⁸ That

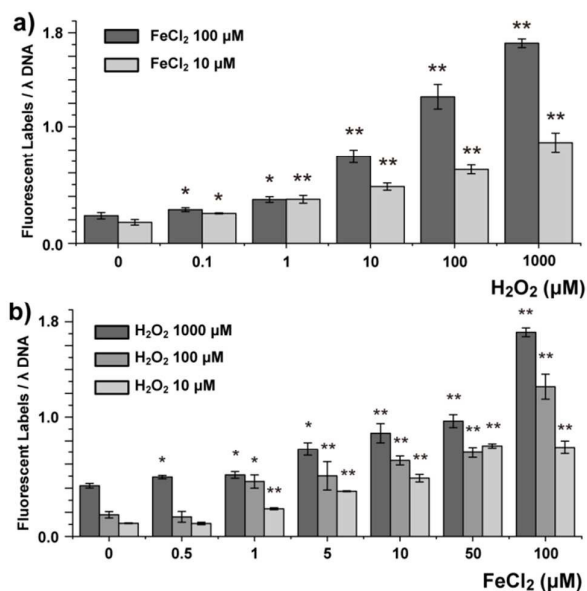


Figure 3. Fenton reaction-induced DNA damage measured at the single molecule level. a) H_2O_2 concentration dependence with two different Fe^{2+} concentrations (dark gray: 100 μM , light gray: 10 μM). b) Fe^{2+} concentration dependence (H_2O_2 : 1 mM dark gray, 100 μM gray, 10 μM light gray). Each data point represents measurement from 100 to 300 molecules; error bars represent standard deviation from three independent trials. (* $p < 0.05$, ** $p < 0.01$ compared with the control)

comparison implied an intriguing insight that DNA sequences themselves in essential genes for capsid and tail may have a tolerance to UV irradiation without any DNA repair enzymes. In a similar context, we searched the literature to find correlation between DNA sequence and oxidative damage, in terms of sensitivity and resistance. Henle *et al.* reported the sequence specific sensitivity for ROS-induced DNA damage.⁴² Their gel electrophoresis result after Fenton reaction showed two strong bands cleaved at a GTGG sequence and another moderate band at an ATGA sequence. From their data, they claimed that RTGR (R represents A or G) might be the consensus sequence for Fenton reaction induced DNA damage. Later, Rai *et al.* explained that sequence selectivity comes from preferential localization of Fe^{2+} ions within the RTGR sequence from NMR structural study.⁴³

To investigate sequence-specific oxidative damage on the genomic map, we first digested λ DNA with restriction enzyme *Xho*I to make two fragments of 33.5 kb and 15 kb before Fenton reaction. This step was critical to find the direction of λ DNA since λ DNA molecules could elongate in two different directions on the surface. In other words, λ DNA can stretch from 5' to 3' as well as from 3' to 5'. Two asymmetric fragments provided directional information for λ DNA genome as shown in Fig. 4a. Fenton reaction and nick translation were followed to generate red-labeled damage spots. In order to compare DNA damage positions with the genomic map, we obtained 350 damaged spots out of 107 λ DNA molecules whose average length were 34.9 pixels (8.7 μm). Thus, we generated *in silico* sequence frequency map by dividing λ DNA genome into 35 segments to match the image resolution for fluorescent images. Figure 4b shows the comparison of our

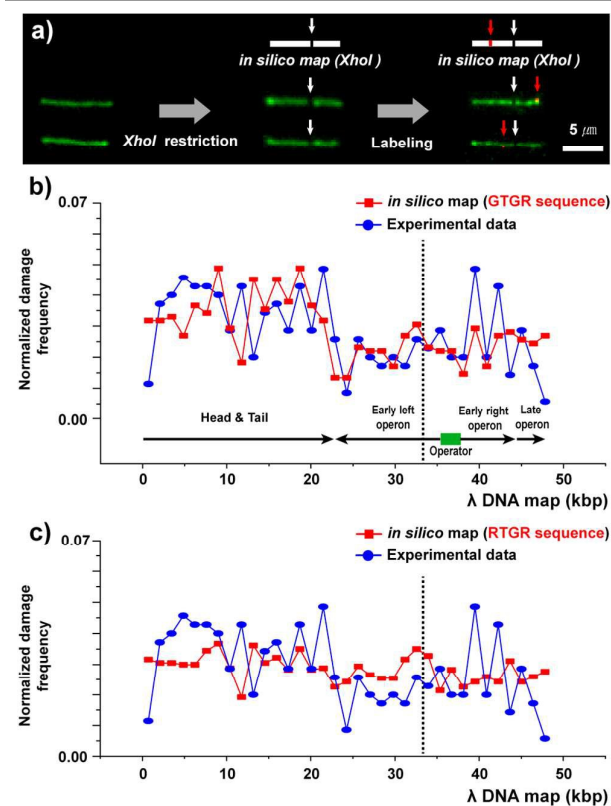


Figure 4. a) Schematic and image of optical mapping based Fenton reaction induced DNA damage. The white arrow represents restricted site by *XhoI* (CTCGAG) to define molecular direction, and the red arrow represents a damaged lesion induced by Fenton reaction at 100 μM H₂O₂ and 100 μM Fe²⁺ (Scale bar: 5 μm). b) Comparison of oxidative damage frequency map (●) and *in silico* GTGR frequency map (■). The dotted line represents *XhoI* cutting site. In this graph, 350 damaged lesions were analysed and λ DNA was divided into 35 segments (48,502/35) to make *in silico* map. c) Comparison of experimental data (●) with *in silico* RTGR frequency map (■). R represents purines (A or G). See supporting information (SI) for other comparison using different sequences.

experimental results (blue circle) with *in silico* sequence frequency maps (red square). Although we attempted to align four types of RTGR sequences (ATGA, ATGG, GTGA, GTGG) with ROS-induced DNA damage, the combination of GTGG and GTGA sequence showed a reasonable correlation as shown in Fig. 4b while RTGR did not show this correlation as shown in Fig. 4c (see SI for more sequence frequency maps). This result suggests that GTGR is the sensitive sequence for oxidative DNA damage. Previously, we reported that essential genes for viral life cycle have fewer thymine dimers, which are a primary target by UV-induced DNA damage.⁸ However, the comparison of ROS-induced DNA damage on the genome map shows an intriguing result that DNA damage frequency and GTGR sequence are noticeably fewer in the early left operon region in the λ genome (Fig. 4b).⁴⁴ Maniatis *et al.* reported that λ genome has four operator sequences of TATCACCGC that lambda repressor (cI) and cro repressor bind, which controls lytic and lysogenic cycles.⁴⁵ As shown in Fig. 4b, P_L and P_R operators exist between 35.6 kb to 38.0 kb. This comparison suggests that low frequency region for ROS-induced damage in the λ DNA genome corresponds to the operator and early left

operon, which regions are primarily active during the lysogenic cycle, when λ DNA is integrated within a host genome. Accordingly, single-molecule DNA damage map implies an interesting biological insight that DNA sequence itself within the genomic map may have sensitivity or resistance to oxidative damage.

Conclusions

Here we demonstrate single molecule analysis of Fenton reaction (Fe²⁺/H₂O₂) induced DNA damage with sensitivity and quantification capability. More importantly, this visualization provides the locations of DNA damage in the DNA backbone. This DNA damage map provides great potential to understand fundamentals of molecular and genetic basis of DNA damage. Furthermore, single molecule DNA analysis for ROS-induced DNA damage will lay the basis for the development of a versatile biosensor to monitor a variety of samples, such as medicine, food, and environmental toxins

Acknowledgements

This work was supported by the Nuclear R&D program and the National Research Foundation of Korea (NRF) grant funded by the MEST (2014R1A2A2A04003870).

Notes and references

1. J. Lee, Y. Kim, S. Lee and K. Jo, *Electrophoresis*, 2015, 36, 2057-2071.
2. D. C. Schwartz, X. Li, L. I. Hernandez, S. P. Ramnarain, E. J. Huff and Y. K. Wang, *Science*, 1993, 262, 110-114.
3. K. Jo, D. M. Dhingra, T. Odijk, J. J. de Pablo, M. D. Graham, R. Runnheim, D. Forrest and D. C. Schwartz, *Proc Natl Acad Sci U S A*, 2007, 104, 2673-2678.
4. E. T. Lam, A. Hastie, C. Lin, D. Ehrlich, S. K. Das, M. D. Austin, P. Deshpande, H. Cao, N. Nagarajan, M. Xiao and P. Y. Kwok, *Nat Biotechnol*, 2012, 30, 771-776.
5. T. T. Perkins, S. R. Quake, D. E. Smith and S. Chu, *Science*, 1994, 264, 822-826.
6. Y. Kim, K. Kim, K. K. L., R. Chang, G. Y. Jung, J. J. De Pablo, K. Jo and D. C. Schwartz, *Lab Chip*, 2011, 11, 1721-1729.
7. J. Lee, S. Kim, H. Jeong, G. Y. Jung, R. Chang, Y. L. Chen and K. Jo, *Acs Macro Lett*, 2014, 3, 926-930.
8. J. Lee, H. S. Park, S. Lim and K. Jo, *Chem Commun*, 2013, 49, 4740-4742.
9. T. Yeom, J. Lee, S. Lee, S. Kang, K. R. Kim, B. Han, H. S. Lee and K. Jo, *Analyst*, 2014, 139, 2432-2439.
10. S. Zirkov, S. Fishman, H. Sharim, Y. Michaeli, J. Don and Y. Ebenstein, *J Am Chem Soc*, 2014, 136, 7771-7776.
11. B. N. Ames, M. K. Shigenaga and T. M. Hagen, *Proc Natl Acad Sci U S A*, 1993, 90, 7915-7922.
12. L. J. Marnett, *Carcinogenesis*, 2000, 21, 361-370.
13. T. B. Kryston, A. B. Georgiev, P. Pissis and A. G. Georgakilas, *Mutat Res*, 2011, 711, 193-201.
14. P. Jezek and L. Hlavata, *Int J Biochem Cell Biol*, 2005, 37, 2478-2503.
15. H. J. H. Fenton, *J Chem Soc Trans*, 1894, 65, 899-910.

ARTICLE

Analyst

16. Y. Z. Luo, Z. X. Han, S. M. Chin and S. Linn, *Proc. Natl. Acad. Sci. U. S. A.*, 1994, 91, 12438-12442.
17. Bruce Alberts, Alexander Johnson, Julian Lewis, Martin Raff, Keith Roberts and P. Walter, *Molecular Biology of the Cell, Fifth Edition*, 2008.
18. J. A. Imlay, S. M. Chin and S. Linn, *Science*, 1988, 240, 640-642.
19. M. Pflaum, O. Will and B. Epe, *Carcinogenesis*, 1997, 18, 2225-2231.
20. A. R. Collins, S. J. Duthie and V. L. Dobson, *Carcinogenesis*, 1993, 14, 1733-1735.
21. A. R. Collins, *Mutat Res*, 2009, 681, 24-32.
22. M. Sharma, *Biochem Biophys Res Commun*, 2000, 273, 40-44.
23. M. V. Vadhanam, J. Thaiparambil, C. G. Gairola and R. C. Gupta, *Chem. Res. Toxicol.*, 2012, 25, 2499-2504.
24. F. Berg, J. Wilken, C. A. Helm and S. Block, *J Phys Chem B*, 2015, 119, 25-32.
25. D. C. Malins and R. Haimanot, *Cancer Res*, 1991, 51, 5430-5432.
26. S. J. London, A. K. Daly, J. B. Leathart, W. C. Navidi, C. C. Carpenter and J. R. Idle, *Carcinogenesis*, 1997, 18, 1203-1214.
27. K. B. Beckman and B. N. Ames, *J. Biol. Chem.*, 1997, 272, 19633-19636.
28. H. Kasai, *Mutat Res-Rev Mutat*, 1997, 387, 147-163.
29. E. T. Dimalanta, A. Lim, R. Runnheim, C. Lamers, C. Churas, D. K. Forrest, J. J. de Pablo, M. D. Graham, S. N. Coppersmith, S. Goldstein and D. C. Schwartz, *Anal Chem*, 2004, 76, 5293-5301.
30. R. A. Bambara, D. Uyemura and T. Choi, *J. Biol. Chem.*, 1978, 253, 413-423.
31. P. W. Rigby, M. Dieckmann, C. Rhodes and P. Berg, *Journal of Molecular Biology*, 1977, 113, 237-251.
32. P. D. Simonson, E. Rothenberg and P. R. Selvin, *Nano Lett*, 2011, 11, 5090-5096.
33. J. A. Imlay, *Annu Rev Biochem*, 2008, 77, 755-776.
34. L. C. Seaver and J. A. Imlay, *Journal of Bacteriology*, 2001, 183, 7182-7189.
35. B. Halliwell, M. V. Clement and L. H. Long, *FEBS Lett.*, 2000, 486, 10-13.
36. S. R. Nelson, A. R. Dunn, S. D. Kathe, D. M. Warshaw and S. S. Wallace, *Proc. Natl. Acad. Sci. U. S. A.*, 2014, 111, E2091-E2099.
37. S. Bjelland and E. Seeberg, *Mutat. Res.-Fundam. Mol. Mech. Mutagen.*, 2003, 531, 37-80.
38. S. Boiteux, E. Gajewski, J. Laval and M. Dizdaroglu, *Biochemistry*, 1992, 31, 106-110.
39. M. Dizdaroglu, J. Laval and S. Boiteux, *Biochemistry*, 1993, 32, 12105-12111.
40. C. Angele-Martinez, C. Goodman and J. Brumaghim, *Metallomics*, 2014, 6, 1358-1381.
41. A. Gupta, M. Place, S. Goldstein, D. Sarkar, S. G. Zhou, K. Potamouis, J. Kim, C. Flanagan, Y. Li, M. A. Newton, N. S. Callander, P. Hematti, E. H. Bresnick, J. Ma, F. Asimakopoulos and D. C. Schwartz, *Proc. Natl. Acad. Sci. U. S. A.*, 2015, 112, 7689-7694.
42. E. S. Henle, Z. Han, N. Tang, P. Rai, Y. Luo and S. Linn, *J Biol Chem*, 1999, 274, 962-971.
43. P. Rai, T. D. Cole, D. E. Wemmer and S. Linn, *J Mol Biol*, 2001, 312, 1089-1101.
44. S. V. Rajagopala, S. Casjens and P. Uetz, *Bmc Microbiol*, 2011, 11.
45. T. Maniatis, M. Ptashne, K. Backman, D. Kield, S. Flashman, A. Jeffrey and R. Maurer, *Cell*, 1975, 5, 109-113.